RESEARCH PAPER

PCCP
www.rsc.org/pccp

Heterogeneous uptake and reactivity of formic acid on calcium carbonate particles: a Knudsen cell reactor, FTIR and SEM study

Hashim A. Al-Hosney, Sofia Carlos-Cuellar, Jonas Baltrusaitis and Vicki H. Grassian*

Department of Chemistry, University of Iowa, Iowa City, Iowa 52246, USA

Received 18th July 2005, Accepted 22nd August 2005
First published as an Advance Article on the web 9th September 2005

The heterogeneous uptake and reactivity of formic acid (HCOOH), a common gas-phase organic acid found in the environment, on calcium carbonate ($CaCO_3$) particles have been investigated using a Knudsen cell reactor, Fourier transform infrared (FTIR) spectroscopy and scanning electron microscopy (SEM). FTIR measurements show that the adsorption of formic acid on the surface of calcium carbonate results in the formation of calcium formate. Besides calcium formate, carbonic acid is also a reaction product under dry conditions (<1% RH). Under dry conditions and at low pressures, the initial uptake coefficient of formic acid on $CaCO_3$ particles is measured to be $3 \pm 1 \times 10^{-3}$ and decreases as the surface saturates with adsorbed products. The maximum surface coverage of formic acid under dry conditions is determined to be $(3 \pm 1) \times 10^{14}$ molecules cm^{-2}. Under humidified conditions (RH >10%), adsorbed water on the surface of the carbonate particles participates in the surface reactivity of these particles, which results in the enhanced uptake kinetics and extent of reaction of this organic acid on $CaCO_3$ as well as opens up several new reaction pathways. These reaction pathways include: (i) the water-assisted dissociation of carbonic acid to CO_2 and H_2O and (ii) the formation of calcium formate islands and crystallites, as evident by SEM images. The results presented here show that adsorbed water plays a potentially important role in the surface chemistry of gas-phase organic acids on calcium carbonate particles.

Introduction

Formic acid and acetic acid are ubiquitous in the atmosphere and are the most abundant organic acids present in urban and remote areas.[1] Together with other carboxylic acids, they contribute up to 64% of the total acidity of precipitation in non-urban environments.[2] Aloisio *et al*[3] determined that organic species like formic acid and acetic acid were significant constituents of atmospheric aerosols; two thirds of the 40% of carbonaceous material found in aerosols were of organic nature. Lee *et al*.[4] measured the chemical components of single particles in the atmosphere and found that 45% of the detected single particles contain a significant amount of organics and oxidized organics. It has been hypothesized that organic acids may be one of the primary sources of cloud condensation nuclei (CCN) in the atmosphere and could make a significant contribution to indirect forcing.[5] Although rain acidity is historically linked to sulfur and nitrogen oxide chemistry, the contribution of organic acids like formic and acetic acid should not be ignored.

Gas-phase concentrations of formic and acetic acid in remote environments are typically in the 0.02–1 ppbv range but can reach up to 16 ppbv in higher polluted urban environments.[6] Major sources of these carboxylic acids include direct anthropogenic and biogenic emissions,[1,7] *in situ* production from precursors in the atmosphere,[8,9] aqueous phase reaction of formaldehyde with OH radical in cloud droplets,[10] gas phase oxidation of non-methane hydrocarbons and aldehydes[11] and photochemical decomposition of isoprene.[9] A continuous flux of organics influences various atmospheric properties including photochemical haze production and the concentration of green house gases.[12]

Carboxylic acids are not significantly removed by gas-phase reactions in the atmosphere due to their relatively low gas phase reactivity. The main gas-phase loss mechanism is the reaction with OH radical.[10] The main removal pathway for these acids from the atmosphere is *via* dry or wet deposition, which accounts for the removal of 95 and 91% of formic and acetic acid, respectively.[13] It is estimated that dry deposition accounts for about half of the removal with deposition velocities measuring on average near 1 cm s^{-1}.[14]

Acidity measurements of atmospheric aerosol reveal that these acids are partially neutralized by alkaline species,[15] which can occur either by particulate matter (*e.g.* $CaCO_3$) or alkaline gases (*e.g.* NH_3). Therefore understanding the heterogeneous chemistry of these acids with the components of atmospheric aerosol is important so that the fate and transport of these gases can be better understood as well as how organic acids contribute to the overall organic composition in atmospheric aerosol.

Calcium carbonate plays a vital role in the chemical regulation of aqueous environments and has been proposed to be an important sink for gas phase inorganic acids like HNO_3.[16] The study of the chemical reactivity of the components of mineral dust aerosol with organic acids like formic acid and acetic acid represents a step in gaining a better understanding of the atmospheric chemistry of these trace organic species. In addition, since calcium carbonate is a ubiquitous mineral and is a component of shells, skeletons, statues and other artwork as well as indoor and outdoor building materials, its reactivity with indoor and outdoor air pollutants will contribute to the deterioration of these materials, as these reactions can lead to the formation of salts that deliquesce at low relative humidity. Acetic acid and formic acid are often found in museum showcases made out of wood, thus represents important gas-phase indoor constituents.[17]

Toward this end, we have investigated the adsorption and reactivity of the simplest organic acid, formic acid, on calcium carbonate particles under different conditions including dry conditions, *i.e.* in the absence of gas phase and adsorbed water, and as a function of relative humidity. Several techniques have been used in this study. These techniques include a Knudsen cell reactor to measure reaction kinetics under dry conditions, transmission and ATR-FTIR spectroscopy to investigate the

DOI: 10.1039/b510112c

adsorption of formic acid under dry and humid conditions, and SEM to determine if the morphology of the particles change with reaction. As discussed in detail below, the results show that adsorbed water plays a potentially important and previously unreported role in the chemistry of gas-phase organic acids on calcium carbonate surfaces.

Experimental

Knudsen cell reactor—principle of operation and experimental apparatus

Knudsen cell reactors are very low-pressure flow reactors that can be used to obtain kinetic information for heterogeneous gas–solid and gas–liquid reactions.[18] The general design of Knudsen cell reactors for the study of heterogeneous reactions has been described in detail in the literature.[18–20] Typically, the reactor consists of a chamber with an isolated sample compartment and a small aperture through which gas-phase reactant and product species can escape to be detected, usually by mass spectrometry. The small volume single stage Knudsen cell reactor used in this study has been described previously.[21] Briefly, the reactor consists of a stainless steel cross that serves as the reaction chamber. The reaction chamber is coupled to an UTI-100C quadrupole mass spectrometer (QMS) through a gate valve. The mass spectrometer is pumped by a 150 l s^{-1} ion pump (Varian). The region between the exit aperture and the gate valve is differentially pumped by a 70 l s^{-1} turbo molecular pump (Varian). Gas molecules are introduced into the reaction chamber through a leak valve. This reactor consists of a stainless steel cube with a volume of 100 cm^3. A single stainless steel sample holder (geometric area of 5.34 cm^2) is covered with a blank flange connected push–pull linear motion feedthrough so the sample holder can be completely and quickly opened by pulling up on the linear motion feedthrough.

Samples for the Knudsen cell experiments were prepared by taking an aqueous slurry of the $CaCO_3$ particles in the small sample holder and allowing the water from this hydrosol to evaporate. This process produces thin films of particles with even coverage of the powdered sample across the bottom of the sample holder, as determined with an optical microscope. The samples were put in the Knudsen reactor and evacuated overnight. Evacuation times were kept constant in order to obtain reproducible data. Since evacuation removes adsorbed water from the surface of the particles, the observation that keeping evacuation times constant is important for a reproducible set of data potentially suggests that adsorbed water may play a role in the uptake of formic acid.

For the Knudsen cell experiments, flowing the reactive gas through the reactor for at least 90 min prior to the experiment passivated the walls of the reactor. The gas was introduced through a leak valve to the desired pressure as measured with an absolute pressure transducer (MKS 690A.1TRC range 10^{-6}–0.1 Torr). During passivation the powdered samples were sealed with the blank flange. The Knudsen cell sample holders have been designed such that there is minimal volume change when the sample lid is opened. Several blank experiments were done in these studies. One set of experiments was done with no sample powder in place to determine if any uptake occurred on the surface of the sample holder. No uptake was observed on the sample holder lid for formic acid when the lid was open without $CaCO_3$ present.

Data analysis for the Knudsen cell reactor experiments

From the Knudsen cell data, an apparent heterogeneous uptake coefficient, γ, which is simply a measure of how likely the molecule will be taken up by the surface, through either adsorption or reaction, per gas-phase collision basis has been measured.

The steady state uptake coefficient for a first order reaction is given in eqn (1):

$$\gamma = \frac{A_h}{A_s}\left(\frac{F_o - F}{F}\right) = \gamma_{obs} \quad (1)$$

In deriving eqn (1) it is typical to use the geometric area of the sample holder, A_s. The term F_o represents the flow of gas in the absence of a reactive surface (*i.e.* when the sample lid is closed to the powdered sample) and F represents the flow of gas in the presence of a reactive surface. Both A_s and A_h are calculated from the measured diameters of the geometric sample holder and the aperture hole, respectively.

Since the measured quantity is usually the mass spectral intensity of the reactant gas and this value is directly proportional to the flow out of the cell, eqn (1) usually appears as

$$\gamma = \frac{A_h}{A_s}\left(\frac{I_o - I}{I}\right) = \gamma_{obs} \quad (2)$$

Here I_o and I are the mass spectral intensities measured in the absence and presence of a reactive surface, respectively. For reasons described below, the uptake coefficient calculated using eqns (2) and (4) will be referred to as the observed uptake coefficient, γ_{obs}.

There are several assumptions made in the derivation of eqns (1) and (2). The first assumption is that the geometric area of the sample holder, A_s, is appropriate in considering the total number of gas-surface collisions. However, for a powdered sample there may be some diffusion into the powder on the time-scale of the measurement (on the order of seconds) and therefore the surface area and thus the number of collisions will be greater than that calculated using A_s. Correcting the observed uptake coefficient for this increased surface area requires an understanding of how gas molecules diffuse into the powder during the time-scale of the measurement.

In 1991, Keyser, Moore, and Leu (KML) adapted a model from the heterogeneous catalysis literature[22] to explain heterogeneous reactions of atmospheric relevance.[23] The model takes into account gas diffusion into the underlying layers of a porous sample by considering the surface area contribution from both the first layer (external) and underlying layers (internal) of particles in determining uptake coefficients.[23,24] As the earlier work includes a complete set of justifications and derivations[22–24] that has been summarized in other publications[25] the details will not be presented here. The premise of the model is that the true uptake coefficient, γ_t, can be thought of in terms of external and internal components which are related to the observed uptake coefficient, γ_{obs} by the following equation

$$\gamma_{obs} = \gamma_t\left(\frac{S_e + \eta S_i}{A_s}\right) \quad \text{where} \quad \eta = \frac{1}{\phi}\tanh(\phi) \quad (3)$$

and

$$\phi = \left(\frac{m}{\rho_b A_s d}\right)\left(\frac{3\rho_b}{2(\rho_t - \rho_b)}\right)(3\tau\gamma_t)^{1/2}$$

The parenthetic term following γ_t is a correction factor for the effect of gas-phase diffusion into the underlying layers. S_i and S_e are the internal and external surface areas, respectively, A_s is the geometric area of the sample holder and η is a calculated 'effectiveness factor'. The effectiveness factor is the fraction of the internal area that contributes to the measured value of the uptake coefficient. Its value is mass (sample thickness) dependent and is determined from the relative rates of surface adsorption and diffusion into the underlying layers. Because of inhomogeneities in the interparticle voids, however, the effective diffusion constant is less than would be calculated

assuming diffusion through long straight capillaries. This effect is accounted for by incorporating a tortuosity factor, τ. Porous solids have predicted τ values in the range of 1–8. However most porous solids, especially powders, are not characterized well enough for an accurate calculation of τ to be made, thus, τ must be experimentally determined. Other parameters in eqn (4) include the mass of the sample, m, the true density of the material, ρ_t, the bulk density of the powder, ρ_b, and the diameter of the particles, d, as discussed in Underwood *et al.*[25]

The form of the equation that we use in our studies is somewhat modified from the work by others in that here we do not assume either simple cubic or hexagonal close-packing spheres. Instead, the experimentally measured bulk density was used in the calculations.[25] In addition, the specific BET surface area was measured rather than calculated. Rewriting eqn (3) in terms of measured bulk density and BET surface area yields

$$\gamma_{obs} = \gamma_t \rho_b S_{BET}(h_e + \eta h_i) \quad (4)$$

where S_{BET} is the BET specific surface area, h_e is the height of the first layer and h_i is the height of all the internal layers calculated from the total mass, the measured bulk density and the particle mass. The data have been fit to this model to determine uptake coefficients.

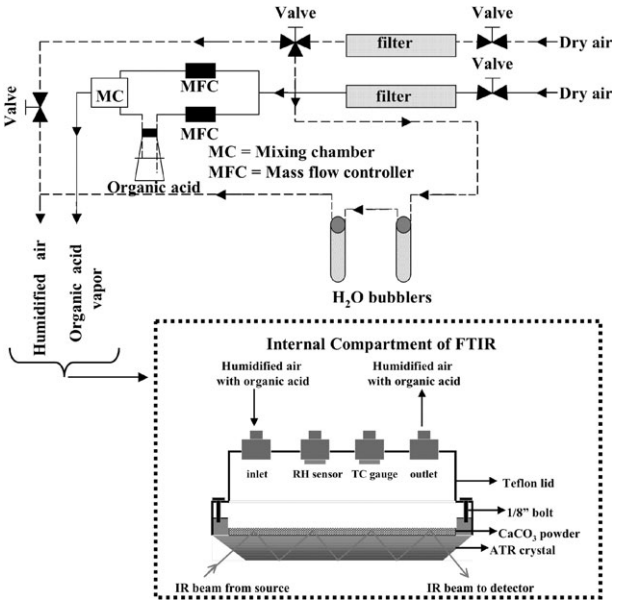

Fig. 1 Schematic diagram of the ATR-FTIR flow cell reactor used to measure relative reaction kinetics as a function of RH.

FTIR measurements

FTIR spectra were recorded using a single beam Mattson Infinity Gold FTIR spectrometer with a liquid-nitrogen-cooled narrow band mercury–cadmium–telluride (MCT) detector. Typically, 250 scans were acquired at a resolution of 4 cm^{-1} over a spectral range of 600–4000 cm^{-1}. For transmission FTIR experiments, approximately 30 mg sample of relatively high surface area $CaCO_3$ was pressed onto one half of a tungsten grid, the other half was uncoated in order to analyze gas-phase species. The tungsten grid was then attached to an infrared cell,[26] mounted onto a linear translator present inside the sample compartment of the FTIR spectrometer. By moving the linear translator into the IR beam path, reaction species and products from the adsorption of gases onto the surface of the pressed powder could be investigated. The infrared cell (164 ± 1 ml) is attached to a glass chamber (1216 ± 4 ml) which is connected to two pressure transducers and a two stage vacuum system consisting of a mechanical pump and a turbo molecular pump that can pump down to 10^{-3} and 10^{-7} Torr, respectively.

A recently designed attenuated total reflection (ATR)-FTIR flow cell reactor was used to measure reaction kinetics as a function of relative humidity.[27] A schematic of the apparatus is shown in Fig. 1. A commercial ATR horizontal liquid cell apparatus (Pike Technology) was modified for these experiments. The optics and ATR cell were placed inside the internal compartment of the spectrometer. Approximately 50 mg of $CaCO_3$ powder were evenly dispersed on an AMTIR (amorphous material transmitting infrared radiation made from a glass containing Ge, As and Se) ATR element. The top plate of the commercial liquid cell was replaced with a Teflon lid. The Teflon lid contained four openings for a relative humidity sensor, a temperature sensor and the remaining two for the humidified air/organic acid inlet and outlet flows. The commercial air dryer used to purge the FTIR spectrometer was used as the air source. As shown in the flow cell schematics, the humidity of the air was controlled by mixing dry and wet air to reach the desired relative humidity as measured by the RH sensor. In a separate line, dry air was saturated with the formic acid vapor. The two air streams, humid air and air containing the organic acid, were sent into the modified commercial ATR cell where the reaction was monitored.

All reported ATR-FTIR spectra were referenced to the AMTIR element containing $CaCO_3$ powder under dry conditions prior to reaction. For kinetic measurements, 180 scans were acquired at a resolution of 8 cm^{-1} over a spectral range of 600–4000 cm^{-1}. The infrared spectra were continuously collected every 2 min to determine relative rates as a function of %RH.

SEM measurements

A Hitachi S-4000 scanning electron microscope was used to acquire images of $CaCO_3$ particles before and after reaction. A Cu transmission electron microscopy finder grid was used in these SEM studies. The grid was fixed to carbon SEM stubs. $CaCO_3$ particles were dispersed onto the carbon stub by placing 2 drops of a dilute solution of methanol containing $CaCO_3$ particles onto the stub and allowing the solution to evaporate. Dilute solutions containing the particles were prepared by mixing approximately 5 mg of $CaCO_3$ with approximately 5 ml methanol and then sonicating this suspension for 2 h before depositing drops onto the stub.

After sample preparation, the $CaCO_3$ particles were imaged with SEM and then transferred in a container to the transmission infrared cell described above so that identical reaction conditions to those used in the infrared experiments could be employed. The stubs containing the particles were placed on the bottom of the IR cell, and the cell was evacuated before water vapor and the organic acid were introduced. Following reaction, the stubs were transferred to the SEM for imaging. Sample imaging before and after reaction was done using a working distance of 10 mm, with an emission current of 10 μA and an accelerating voltage of 2.5 kV.

Sources of powders and gases

Two different $CaCO_3$ samples were used in these experiments. For the Knudsen cell reactor and SEM studies, low surface area $CaCO_3$ purchased from Alfa Aesar with a surface area of 1.4 $m^2\ g^{-1}$ was used. For the infrared studies, a higher surface area $CaCO_3$ sample purchased from OMYA with a surface area of 10.4 $m^2\ g^{-1}$ was used. The vapor above liquid formic acid [Fluka Chemika, 98% purity] and distilled water (Optima water from Fisher Scientific) were used in this study. All liquids were degassed *via* several freeze–pump–thaw steps prior to use.

Results

Heterogeneous uptake of formic acid on calcium carbonate: Knudsen cell reactor measurements

The heterogeneous uptake of gas-phase formic acid on $CaCO_3$ is shown in Fig. 2. The Knudsen cell data, plotted as QMS intensity of the parent ion for formic acid ($m/z = 46$) as a function of time, are shown in Fig. 2a. As discussed in the Experimental section, a steady state flow is established in the reactor before the experiment begins. The formic acid pressure in the Knudsen cell reactor was kept at 6 μTorr corresponding to a gas concentration of 1.9×10^{11} molecules cm^{-3}. Four different experiments with different $CaCO_3$ sample mass are shown in Fig. 2a for uptake of formic acid. It can be seen that there is a decrease in the QMS signal when the sample is exposed to gas-phase formic acid. The abrupt drop in the QMS signal occurs when the sample lid is open and when the particles are first exposed to formic acid. The uptake decreases as a function of time and for the sample with the smallest mass, the first experiment shown in Fig. 2a, the sample saturates with the formic acid over the time of the experiment. In the data shown in Fig. 2a, the carbonate samples are exposed to formic acid for ~180 s. It can be seen when the sample lid is closed, the signal goes back to its original baseline value.

The observed uptake coefficient for the heterogeneous uptake of formic acid on calcium carbonate can be determined from the data shown in Fig. 2a. The observed uptake coefficients calculated using eqn (2) for formic acid are shown in Fig. 2b for the different calcium carbonate samples. The values of A_h and A_s used in the calculation are given in the figure caption. The data show that the observed uptake coefficient, γ_{obs}, decreases as calcium carbonate is exposed to these organic acids. The decrease in the uptake coefficient occurs because the surface becomes saturated with adsorbed molecules. Since the uptake coefficient is coverage and thus time dependent, it is typical to report an initial uptake coefficient. The data shown in Fig. 2b show that the value of the initial uptake coefficient depends on the mass of the sample.

These mass dependent data can be used to calculate a true uptake coefficient. The data plotted in Fig. 3 show the observed initial uptake coefficient determined for heterogeneous uptake of formic acid on calcium carbonate as a function of sample mass. The data include the experiments shown in Fig. 2 as well as some additional experiments. The data points are shown as solid circles and a fit to the data using the diffusion model discussed in the Experimental section is shown in Fig. 3 as well. The experimental data were fit using a non-linear least squares fitting routine. The experimental parameters used in the model are given in the figure caption as well as the fitting parameters, the true initial uptake coefficient, $\gamma_{o,t}$ and the tortuousity, τ. For heterogeneous uptake of formic acid on $CaCO_3$, the true initial uptake coefficient under dry conditions present in the Knudsen cell is determined to be $3 \pm 1 \times 10^{-3}$, with the error in the measurement estimated from the uncertainty in the parameters and the scatter in the data points. The major uncertainty in these measurements is often related to knowing the effective surface area.[21]

To determine if adsorption of these organic acids is reversible or irreversible, Knudsen cell extraction experiments were done. In these experiments, after the surface had become saturated or equilibrated with the gas phase, the lid was

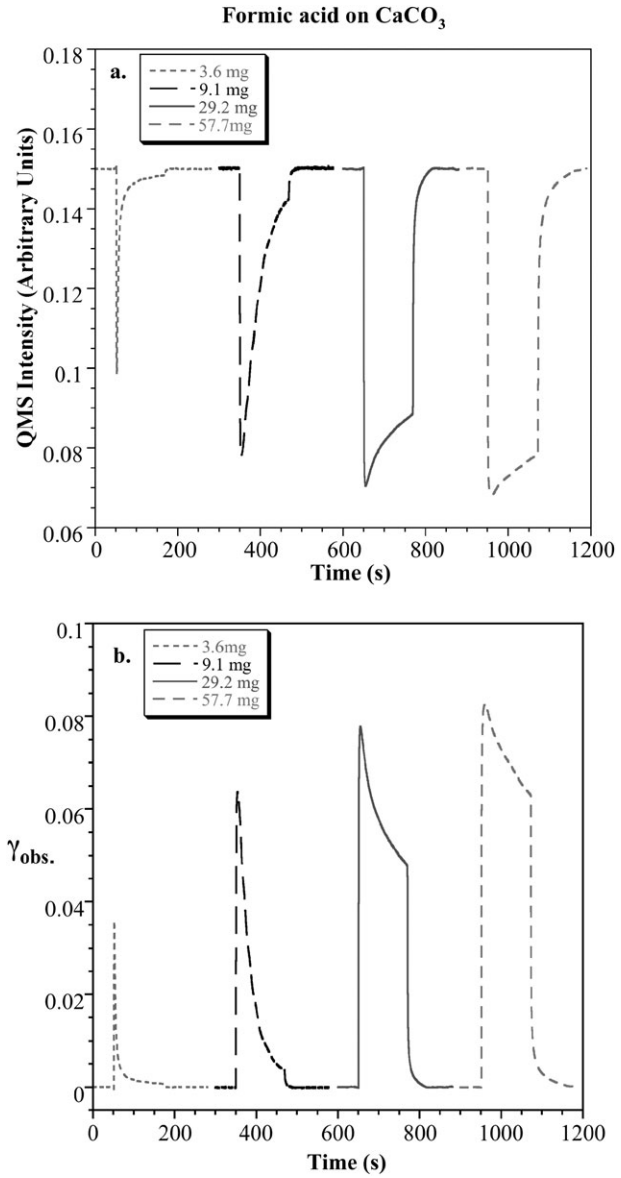

Fig. 2 (a) QMS intensity ($m/z = 46$) plotted as a function of time for formic acid uptake on $CaCO_3$ powder (BET surface area of 1.4 m^2 g^{-1}) of various mass. Four different experiments are shown on the graph and displaced from each other along the x-axis. (b) Calculated observed uptake coefficient for the data shown in (a) using eqn (2) with $A_h = 0.363$ cm^2 and $A_s = 5.34$ cm^2.

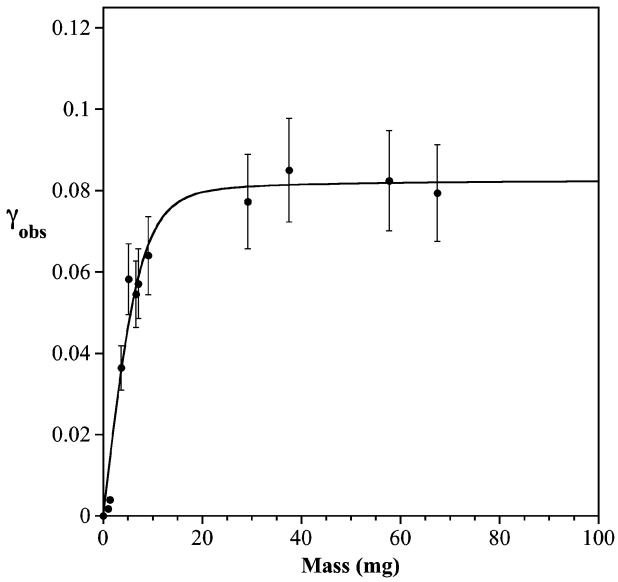

Fig. 3 Initial uptake coefficients calculated using eqn (2) are plotted as a function of sample mass for formic acid uptake on $CaCO_3$, at a formic acid concentration of 1.9×10^{11} molecules cm^3. The lines through the data points represent a best fit of the data to eqns (3) and (4) and the following experimental and fitting parameters: $S_{BET} = 1.4$ m^2 g^{-1}; $d = 2.7$ μm; $\rho_b = 0.76$ g cm^{-3}; $\rho_t = 2.93$ g cm^{-3}; $\tau = 4$ and $\gamma_{o,t} = 2.7 \times 10^{-3}$.

lowered to cover the oxide and the leak valve was turned off so that the gas was pumped out by the two stage pumping system described in the Experimental section. After formic acid was evacuated from the Knudsen cell reactor system, the sample lid was then raised while the QMS monitored for the desorption of formic acid from the surface. It was determined that a small amount of the acid desorbed back into the gas phase (*ca.* 2%) whereas the majority of the formic acid was irreversibly adsorbed. In order to learn more about the surface adsorbed products, the adsorption of formic acid on $CaCO_3$ was further investigated by transmission FTIR spectroscopy.

Heterogeneous uptake of formic acid on calcium carbonate: transmission FTIR measurements

Fig. 4a shows the infrared spectrum recorded after calcium carbonate particles were exposed to formic acid (270 mTorr) for 30 min under dry conditions at 0% RH. This spectrum and the one shown in Fig. 4b were referenced to the $CaCO_3$ particles prior to formic acid exposure. Under these conditions, the $CaCO_3$ particles become saturated with adsorbed products and do not take up any additional formic acid. Volumetric measurements were used to determine that the saturation coverage is $3 \pm 1 \times 10^{14}$.[27] The spectrum shown in Fig. 4a was recorded following evacuation of the gas phase.

The spectrum shows that upon evacuation of gas-phase formic acid, absorption bands remain in the spectrum indicating that adsorbed products remain on the surface. Before assigning the bands in the spectrum shows in Fig. 4a, it is useful to see what changes occur upon water adsorption at high relative humidity near 94% RH. Fig. 4b shows a spectrum recorded after $CaCO_3$ particles were first exposed to formic acid and then exposed to 94% RH for 30 min. Prior to recording the spectrum shown in Fig. 4b, the water vapor was evacuated from the infrared cell. It can be seen that the spectrum is changed from that shown in Fig. 4a. In particular, there is a change in vibrational frequency and intensity of some of the bands as well as the complete loss of several of the absorption bands.

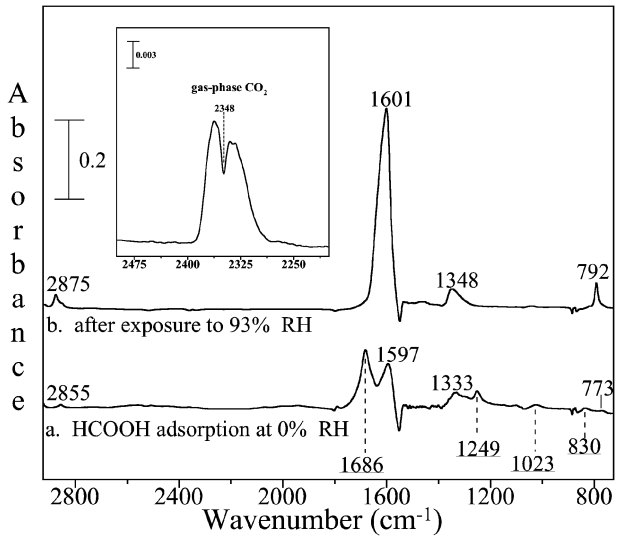

Fig. 4 (a) Transmission FTIR spectra recorded of $CaCO_3$ particles following exposure to HCOOH (270 mTorr) under dry conditions. The spectrum can be assigned to adsorbed carbonic acid and adsorbed formate (see Tables 1 and 2, respectively). The frequencies of the absorption bands associated with adsorbed carbonic acid are underlined so as to differentiate carbonic acid bands from formate bands. (b) The $CaCO_3$ particles were then exposed to higher relative humidity (94% RH) following exposure to formic acid. Several changes are observed in the spectrum following exposure to water, shifts in frequency and intensity are seen for some of the absorption bands whereas others disappear completely from the spectrum. The absorption bands associated with adsorbed carbonic acid are seen to disappear due to the catalyzed dissociation of this adsorbed product in the presence of adsorbed water. See text for further details.

As discussed in detail here, the spectra shown prior to water adsorption (Fig. 4a) can be assigned to the presence of adsorbed formate on the $CaCO_3$ surface following reaction with formic acid, along with adsorbed carbonic acid which is unstable in the presence of adsorbed water. The surface reaction associated with this chemistry is shown in reaction (5).

$$Ca(OH)(HCO_3)(s) + HCOOH(g) \rightarrow Ca(OH)(HCOO)(a) + H_2CO_3(a) \quad (5)$$

The surface of calcium carbonate single crystals has been shown by X-ray photoelectron studies to contain a thin layer of hydroxides and bicarbonate species formed by the dissociative adsorption of water.[28] Water dissociation on the $CaCO_3$ surface results in a surface stoichiometry best represented as $Ca(OH)(HCO_3)$. Since the particles used in these studies have been exposed to air, formic acid reacts with $Ca(OH)(HCO_3)$, to yield the two adsorbed products—formate and carbonic acid. The negative feature near 1552 cm^{-1} is in fact due to the loss of the bicarbonate (HCO_3^-) from the surface upon reaction with formic acid, according to (5).

Adsorbed carbonic acid has been previously observed with infrared spectroscopy as it also forms following reaction of nitric acid with calcium carbonate particles under dry conditions. The absorption bands in the spectrum shown in Fig. 4a at 1686, 1249, 1023 and 830 cm^{-1} are assigned to adsorbed carbonic acid. The most intense band at 1686 cm^{-1} is assigned to the C=O stretch. The detailed vibrational mode assignment for adsorbed carbonic acid is given in Table 1 and agrees well with previously reported results as the assignment for adsorbed carbonic acid has been thoroughly discussed in previous publications.[29–32]

As discussed previously, the dissociation of carbonic acid to water and carbon dioxide is catalyzed by water. Theoretical studies have shown that the rate of dissociation of gas-phase carbonic acid increases by a factor of 10^8 when one water molecule is present.[33] Adsorbed carbonic acid has previously been reported to be similarly destabilized in the presence of adsorbed water and thus its disappearance upon exposure to 94% RH is consistent with this. The inset of Fig. 4 shows the spectrum of the gas phase in the region of the spectrum where CO_2 absorptions are expected, in the presence of 94% RH. It can be seen that gas-phase CO_2 is present in the spectrum consistent with the dissociation of carbonic acid, gas-phase water is also present (spectral regions for O–H stretching and bending modes not shown) as the spectrum was recorded at 94% RH. It is important to note that the gas-phase CO_2 absorption band is not present when water vapor alone is added to the infrared cell in the presence of unreacted $CaCO_3$.

The remaining bands in the spectrum shown in Fig. 4a can be assigned with the aid of previous infrared studies of crystalline calcium formate[34–36] and following the reaction of formic acid on metal[37] and metal oxides[38–41] to adsorbed formate. The band at 2855 cm^{-1} is assigned to the C–H stretch, ν(C–H), the band at 1597 cm^{-1} is assigned to the asymmetric carboxylate stretch, ν_a(OCO), the band at 1333 cm^{-1} is assigned to the symmetric carboxylate stretch, ν_s(OCO), and the band at 773 cm^{-1} is assigned to the carboxylate deformation mode, δ(OCO). After the surface is exposed to adsorbed water the vibrational bands of adsorbed formate change in intensity and shift in frequency. These spectral changes suggest that the environment of the formate group is different after exposure to adsorbed water. SEM images (*vide infra*) show that microcrystallites of calcium formate form in the presence of water. These new structures most likely provide an environment more similar to that of the crystalline salt than to an adsorbed monolayer. Additional experiments of formic acid reaction

Table 1 Vibrational mode assignment of adsorbed carbonic acid, H_2CO_3, a product in the reaction of HCOOH on $CaCO_3$

Vibrational mode	Frequencies observed for adsorbed H_2CO_3 from HCOOH adsorption	Frequencies observed for adsorbed H_2CO_3 from HNO_3 adsorption [ref 32]	Frequency for condensed H_2CO_3 [ref. 29–31]
C═O stretch, ν(C═O)	1686	1685	1705
COH in-plane bend, δ(CO–H)	1249	1270	1296
$C(OH)_2$ symmetric stretch, ν(C–O)	1023	1021	1034
CO_3^{2-} out-of-plane bend, $\delta(CO_3^{2-})$	830	837	812

Table 2 Vibrational mode assignment for surface adsorbed formate and calcium formate crystallites following reaction of HCOOH on $CaCO_3$ under dry conditions and in the presence of water vapor, respectively

Vibrational mode	Frequencies (cm^{-1}) for adsorbed formate (dry conditions)	Frequencies (cm^{-1}) for calcium formate microcrystallites (presence of water vapor)
C–H stretch, ν(C–H)	2855	2875
OCO asymmetric stretch, ν_{as}(OCO)	1597	1601
OCO symmetric stretch, ν_s(OCO)	1333	1348
OCO deformation mode, δ(OCO)	773	792

on calcium carbonate in the presence of water are discussed below.

Heterogeneous uptake of formic acid on calcium carbonate at higher relative humidity: transmission and ATR-FTIR measurements

As discussed above, there is evidence that adsorbed water plays a role in the surface chemistry of formic acid on calcium carbonate. Further experiments to investigate the role of water in the reaction of calcium carbonate with formic acid are presented here. In particular, the reaction of calcium carbonate particles with formic acid when simultaneously exposed to the organic acid and water vapor is discussed.

The adsorption of formic acid on calcium carbonate particles in the presence of water as a function of relative humidity is shown in Fig. 5. The bottom spectrum shows the data following adsorption of formic acid on calcium carbonate at a pressure of 270 mTorr for 30 min. The other spectra shown in Fig. 5 result from the exposure of the same amount of formic acid with increasing %RH after 30 min equilibration time. This procedure was repeated until 94% RH was reached. Each spectrum was recorded following evacuation of the formic acid/water vapor mixture. It can be seen that the peaks associated with calcium formate are observed to increase in intensity and shift in frequency. At the highest relative humidity band frequencies are at 2875 cm^{-1} (ν(C–H)), 1601 cm^{-1} (ν_{as}(OCO)), 1348 cm^{-1} (ν_s(OCO)), and 792 cm^{-1} (δ(OCO)). The inset of Fig. 5 shows relative changes in the integrated absorbance of the asymmetric OCO stretch. The integrated absorbance for the 0% RH experiment is normalized to one. It can be seen that the amount of formate increases at higher relative humidity. The 1601 cm^{-1} (ν_{as}(OCO)) is generally found to be the most intense component of the vibrational spectrum in formate salts[35] and is the most intense band here due to the formation of crystalline calcium formate on the surface (*vide infra*). Other bands also increase in intensity but their growth trends vary. For example, the band near 792 cm^{-1} is initially quite weak until higher %RH and then it becomes more distinct and of higher intensity at its peak compared to the 1348 cm^{-1} band. These different growth patterns may be related to the formation of different structures of calcium formate on the surface (*e.g.* surface adsorbed, amorphous phase or crystalline phase) that have slightly different vibrational frequencies.

This enhanced uptake in the presence of adsorbed water suggests that additional adsorption sites become available for reaction in the presence of adsorbed water. In the presence of adsorbed water, the reaction involves underlying layers and a net reaction can be written as

$$CaCO_3(s) + 2HCOOH(g) \rightarrow Ca(HCOO)_2(s) + CO_2(g) + H_2O(a) \quad (6)$$

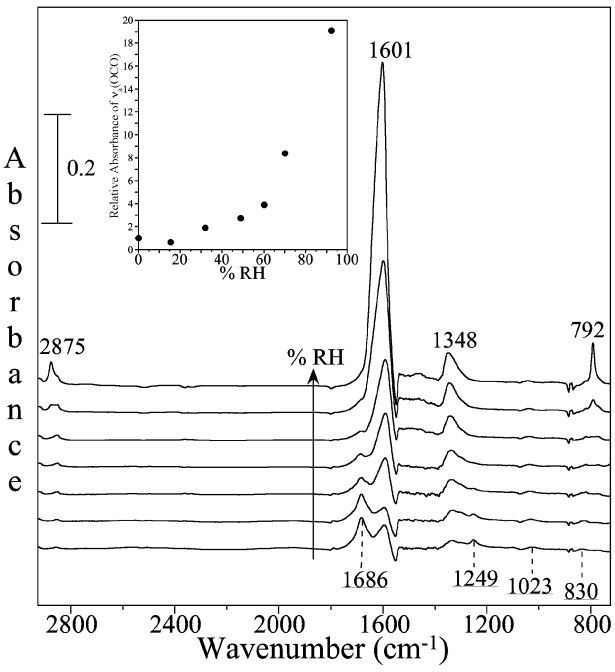

Fig. 5 FTIR spectra following the simultaneous adsorption of formic acid (270 mTorr) as a function of relative humidity (0, 15, 32, 49, 60, 70, and 94% RH). Each spectrum was recorded after evacuation of the formic acid/water vapor mixture. Inset: Normalized integrated absorbance of the ν_a(OCO) mode of adsorbed acetate as %RH is increased. Two conclusions can be made from these infrared data. The first is that absorption bands due to adsorbed carbonic acid decrease in intensity at higher relative humidity. The second is that the amount of adsorbed formate increases significantly as a function of relative humidity as indicated by the increase in the absorption bands at 2875, 1601, 1348 and 792 cm^{-1}.

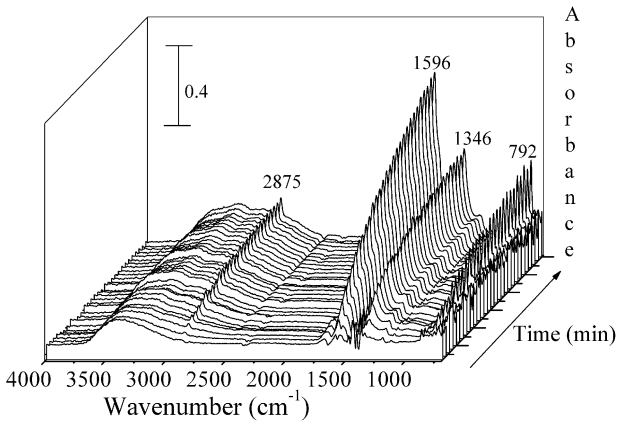

Fig. 6 Time-course ATR-FTIR spectra are shown above. These spectra were collected using the flow apparatus shown in Fig. 1. The first 50 min of data collection are shown. The ATR-FTIR spectra were recorded in the presence of water vapor corresponding to 35% RH and a pressure of formic acid of 600 mTorr.

The relative rate of formate formation was also examined as a function of relative humidity in the ATR-FTIR flow cell reactor shown in Fig. 1. In these experiments, the formic acid pressure was kept constant and the relative humidity was varied. Three experiments were done at 0, 35 and 62% RH. The time course ATR-FTIR spectra collected for 50 min are shown in Fig. 6. These data show that the absorption bands due to adsorbed formate increase as a function of time. The C–H stretching mode is seen to be on the broad O–H stretching absorption due to adsorbed water on the calcium carbonate surface.[28] The formate absorptions in the ATR-FTIR spectra are seen to be slightly shifted by a few wavenumbers from the transmission spectra.

The spectra also show that the rate of increase is reduced at the longer times as the spectra taken after 20 min show a leveling off of the formate absorption bands. It was determined that the absorption bands show a linear increase in intensity only for the first 10 to 20 min of the experiment. Fig. 7 shows a plot of integrated area of the asymmetric OCO stretch (ν_a (OCO)) of adsorbed formate as a function of time. It can be seen from the data shown in Fig. 7 that the rate of formate formation increases as a function of relative humidity. The relative rates taken as the slope of the lines shown in Fig. 7 normalized to the rate at 0% RH are 1, 3.6 and 7.0 for 0, 35

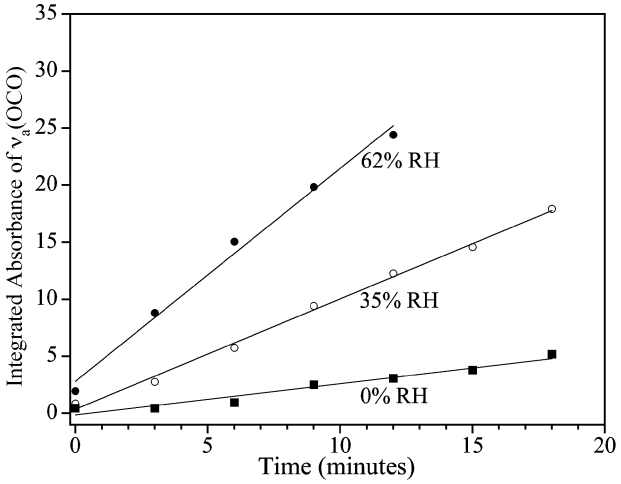

Fig. 7 The relative rate of formation of adsorbed formate is shown following reaction of formic acid at different relative humidity. The integrate absorbance is plotted as a function of time. The growth of the absorption band is seen to be linear in the first *ca.* 20 min. The slopes of these lines are seen to increase as a f(RH). The relative slopes are 1, 3.6, and 7.0 for 0, 35 and 62% RH, respectively.

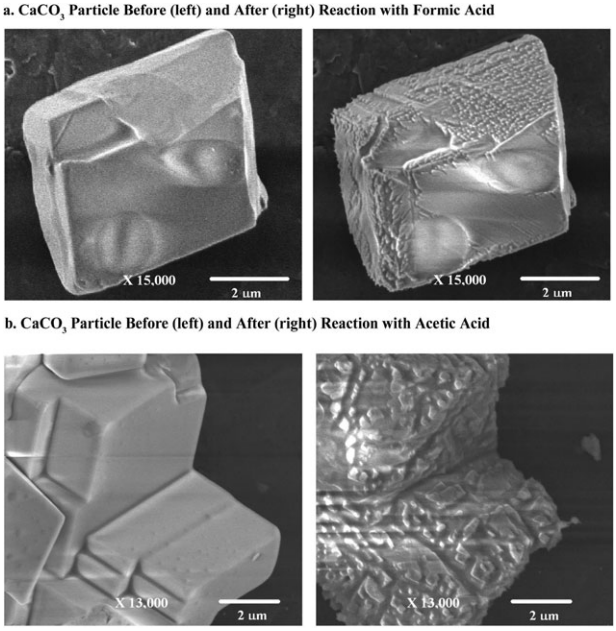

Fig. 8 (a) SEM images of calcite particles before (left) and after (right) reaction with formic acid in the presence of water vapor corresponding to 80% RH. Following reaction, the particle shows the formation of calcium formate crystals on the carbonate particle. (b) Similar results are seen for reaction of acetic acid on $CaCO_3$ to form calcium acetate crystals.

and 62% RH, respectively. That is to say that the rate becomes nearly an order of magnitude greater at the highest relative humidity. Thus rates of reactions involving atmospheric gases will depend on relative humidity similar to what was found for nitric acid.[42]

Heterogeneous uptake of formic acid on calcium carbonate at higher relative humidity: SEM measurements

The above infrared studies show that the reaction of $CaCO_3$ with formic acid is enhanced in the presence of water vapor. In particular, there is no apparent surface saturation for reactions of formic acid on $CaCO_3$ at higher relative humidities. These results are similar to that found with the reaction of HNO_3 and SO_2 on $CaCO_3$.[32] In the case of HNO_3, it has been shown that the calcium nitrate product forms a deliquescent film above 10% RH.[43–46] This deliquescent layer is thought to enhance the reactivity of HNO_3 on $CaCO_3$. In the case of SO_2, it was proposed that calcium sulfite islands and microcrystals formed at higher relative humidity in the presence of adsorbed water. The formation of islands and microcrystallites of $CaSO_3$ would expose sites on the $CaCO_3$ surface that would allow for continued reactivity. Recently, the formation of islands and microcrystallites of $CaSO_3$ has been identified with SEM images.[27]

The formation of calcium formate islands and crystallites on reacted $CaCO_3$ particles was investigated with SEM in this study. Fig. 8 shows images of a $CaCO_3$ particle before and after reaction with formic acid. It can be seen that the unreacted particle has smooth surfaces and edges. For the reacted particle, there are small features on the surfaces and at the edges that are approximately 10–100 nm in size. These nanometer features are proposed to be islands and microcrystallites of calcium formate.

The particle in Fig. 8 was reacted for 20 h and the image shows that there are many microcrystallites on the particle surface. If the particle is reacted for less time or at lower formic acid pressures, microcrystallites have been shown to form in the same size range but there are much fewer of them. These features indicate that phase segregation of the reaction

Table 3 Vibrational frequencies for three different phases of crystalline calcium formate[a] compared to the vibrational frequencies of the microcrystallites formed from reaction of formic acid on $CaCO_3$

Vibrational mode	α-$Ca(HCOO)_2$	β-$Ca(HCOO)_2$	γ-$Ca(HCOO)_2$	This work
C–H stretch, ν(C–H)	2869	2880	2875	2875
OCO asymmetric stretch, ν_{as}(OCO)	1587	1600	1600	1601
OCO symmetric stretch, ν_s(OCO)	1353	1359	1356	1348
OCO deformation mode, δ(OCO)	789	791	791	792

[a] From refs. 34–36.

product, in this case calcium formate, in the presence of adsorbed water readily occurs. There are several crystalline forms of calcium formate that are known. The alpha structure, α-$Ca(HCOO)_2$, is orthorhombic while the beta structure, β-$Ca(HCOO)_2$ is tetragonal.[35] The α-form crystallizes from aqueous solution and the β-form crystallizes when a water miscible organic solvent is added into an aqueous solution of $Ca(HCOO)_2$.[34] Another form, γ-$Ca(HCOO)_2$, is stable at higher temperatures in the temperature range 150–220 °C, but transforms into β-$Ca(HCOO)_2$ on cooling and in the presence of water vapor the β-$Ca(HCOO)_2$ transforms into α-$Ca(HCOO)_2$.[36] The vibrational frequencies for these three crystalline structures are given in Table 3. Based on the frequencies of these three crystalline forms and the frequencies observed for the calcium formate microcrystals formed by reaction of formic acid with $CaCO_3$, it is seen that the agreement is best for the gamma form at the highest RH shown in Fig. 5. This suggests that a higher energy form may be stable for these small crystallites supported on $CaCO_3$. One proposal is that the calcium formate product changes from an adsorbed surface layer, possibly to an amorphous phase, and then to a higher energy crystalline phase as the extent of reaction increases as a f(RH). This type of transformation in which higher energy metastable phases form initially is consistent with a growth process controlled by kinetics and follows the Ostwald rule of stages (Ostwald step rule).[47–49] The essence of the rule of stages is that a system does not go directly to the most stable conformation corresponding to the lowest free energy but prefers to reach intermediate stages of free energy closes to the initial stage. This growth mechanism is quite common in geochemical systems[50] and thin film growth.[51]

Similar studies for acetic acid also show that islands and microcrystallites form (see Fig. 8b). In this case, these islands and microcrystallites are due to calcium acetate hydrate.[27] Thus it can be concluded from the SEM images that ionic

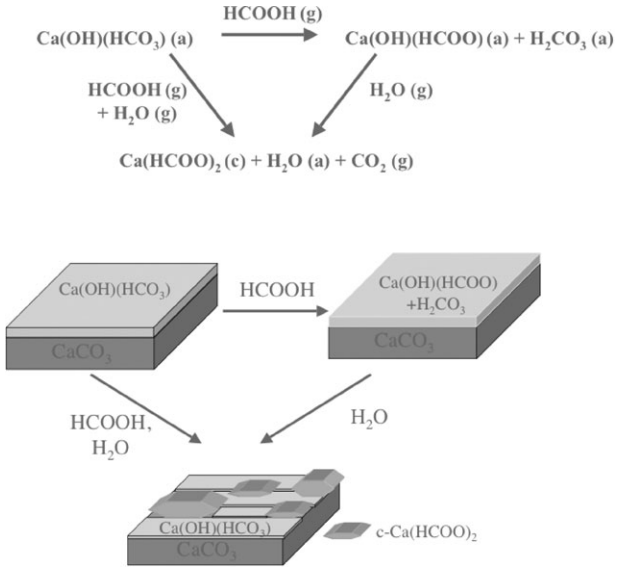

Scheme 1 Surface reactions of formic acid on calcium carbonate.

mobility, phase segregation and crystallite formation are important for reactions involving organic acids on calcium carbonate surfaces under ambient conditions of temperature and relative humidity.

From this combined Knudsen cell reactor, FTIR and SEM study, a picture begins to emerge for the reaction of formic acid on $CaCO_3$ particles and the influence of adsorbed water in this reaction. The pertinent reactions and pictorial cartoon of the formation of surface islands and microcrystals are shown in Scheme 1 (not balanced). Adsorbed water has two important roles with respect to the reaction mechanism. First, adsorbed water catalyzes the decomposition of carbonic acid. Second, adsorbed water enhances the mobility of the surface ions to facilitate the formation of the calcium formate 3-D structures and exposes new sites on the $CaCO_3$ surface for continued reactivity. The formation kinetics of calcium formate microcrystals are enhanced in the presence of water as shown by the ATR-FTIR flow cell experiments.

Conclusions

Several interesting conclusions can be made from this study on the adsorption of formic acid on $CaCO_3$ under different conditions of relative humidity.

(i) Under dry conditions, formic acid adsorbs with initial heterogeneous uptake coefficient of $3 \pm 1 \times 10^{-3}$. The uptake coefficient decreases as a function of exposure time until no more uptake is observed.

(ii) The adsorption of formic acid on the surface of calcium carbonate under dry conditions results in the formation of adsorbed formate. Another product that forms in the reaction is identified as adsorbed carbonic acid, H_2CO_3.

(iii) These products strongly adsorb on the surface providing a capping layer that inhibits additional uptake of formic acid. The saturation coverage of adsorbed formic acid under dry conditions is determined to be $3 \pm 1 \times 10^{14}$.

(iv) Adsorbed carbonic acid dissociates into CO_2 and H_2O in the presence of adsorbed water.

(v) At higher relative humidity, formic acid can react to a greater extent with $CaCO_3$ without undergoing surface saturation indicating that underlying layers are participating in the reaction and ionic mobility is enhanced in the presence of adsorbed water.

(vi) SEM images of the particles following reaction of formic acid at higher relative humidity show that in the presence of water calcium formate phase segregates and forms crystallites.

(vii) At higher relative humidity, the heterogeneous reaction kinetics increases. At 62% relative humidity the rate increases nearly an order of magnitude compared to dry conditions near 0% RH indicating that the rate as well as the extent of the reaction increases with increasing relative humidity.

Acknowledgements

The authors greatly appreciate the support of the National Science Foundation through a creativity extension of CHE-9984344 and CHE-0503854.

References

1 D. Grosjean, *Environ. Sci. Technol.*, 1989, **23**, 1506.
2 W. C. Keene, J. N. Galloway and J. D. Holden, *J. Geophys. Res.*, 1983, **88**, 5122.
3 S. Aloisio, P. E. Hintze and V. Vaida, *J. Phys. Chem. A*, 2002, **106**, 363.
4 S. H. Lee, D. M. Murphy, S. D. Thomson and A. M. Middlebrook, *J. Geophys. Res.*, 2003, **108**, 5.
5 S. Yu, *Atmos. Res.*, 2000, **53**, 185–217.
6 A. K. Haider, *Atmos. Environ.*, 1995, **29**, 127.
7 R. W. Talbot, K. M. Beecher, R. C. Harris and W. R. Cofer III., *J. Geophys. Res.*, 1988, **83**, 1638.
8 J. G. Calvert and S. Madrinich, *J. Geophys. Res.*, 1987, **92**, 2211.
9 D. J. Jacob and S. C. Wosley, *J. Geophys. Res.*, 1988, **93**, 1477.
10 A. Chebbi and P. Carlier, *Atmos. Environ.*, 1996, **30**, 4233.
11 F. Su, J. G. Calvert and J. H. Shaw, *J. Phys. Chem.*, 1979, **83**, 3185.
12 M. J. Adams, J. V. H. Constable, A. B. Gunther and P. Zimmerman, *Chemosphere*, 2001, **3**, 73.
13 D. Grosjean, *Atmos. Environ.*, 1992, **26A**, 3279.
14 P. Khare, N. Kumar, K. M. Kumari and S. S. Srivastava, *Rev. Geophys.*, 1999, **37**, 227.
15 F. Adalgiza and I. G. R. Gutz, *Atmos. Environ.*, 2003, **37**, 117.
16 A. Tabazadeh, M. Z. Jacobson, H. B. Singh, O. B. Toon, J. S. Lin, R. B. Chatfield, A. N. Thakur, R. W. Talbot and J. E. Dibb, *Geophys. Res. Lett.*, 1998, **25**, 4185.
17 A. V. Dremetsika, P. A. Siskos and E. B. Bakeas, *Indoor Built Environ.*, 2005, **14**, 51.
18 D. M. Golden, G. N. Spokes and S. W. Benson, *Angew. Chem., Int. Ed. Engl.*, 1973, **12**, 534.
19 F. Caloz, F. F. Fenter, K. D. Tabor and M. J. Rossi, *Rev. Sci. Instrum.*, 1997, **68**, 3172.
20 D. M. Golden and J. A. Manion, *Advances in Chemical Kinetics and Dynamics*, JAI Press, 1992, vol. 1 187.
21 E. R. Johnson, J. Scieglenka, S. Carlos-Cuellar and V. H. Grassian, *J. Phys. Chem. A*, 2005, **109**, 6901.
22 R. Aris, *The Mathematical Theory of Diffusion and Reactions in Permeable Catalysts*, Clarendon Press, Oxford, 1975, vol. I.
23 L. F. Keyser, S. B. Moore and M.-T. Leu, *J. Phys. Chem.*, 1991, **95**, 5496.
24 L. F. Keyser, M.-T. Leu and S. B. Moore, *J. Phys. Chem.*, 1993, **97**, 2800.
25 G. M. Underwood, P. Li, C. Usher and V. H. Grassian, *J. Phys. Chem. A*, 2000, **104**, 819.
26 V. H. Grassian, *J. Phys. Chem. A*, 2002, **106**, 860.
27 H. A. Al-Hosney, Ph.D. Thesis, University of Iowa, 2005.
28 S. L. S. Stipp and M. F. Hochella, Jr., *Geochim. Cosmochim. Acta*, 1999, **55**, 1723.
29 W. Hage, A. Hallbrucker and E. Mayer, *J. Am. Chem. Soc.*, 1993, **115**, 8427.
30 M. H. Moore and R. K. Khanna, *Spectrochim. Acta*, 1991, **47A**, 255.
31 J. R. Brucato, M. E. Palumbo and G. Strazzulla, *Icarus*, 1997, **125**, 135.
32 H. A. Al Hosney and V. H. Grassian, *Phys. Chem. Chem. Phys.*, 2005, **7**, 1266.
33 T. Loerting, c. Tautermann, R. T. Kroemer, I. Kohl, A. Hallbrucker, E. Mayer and K. R. Liedl, *Angew. Chem., Int. Ed.*, 2000, **39**, 891.
34 C. J. H. Schutte and K. Buijs, *Spectrochim. Acta*, 1964, **20**, 187.
35 S. D. Ross, *Inorganic Infrared and Raman Spectra*, McGraw Publishing, 1972.
36 B. F. Mentzen and C. Comel, *Spectrochim. Acta*, 1974, **30**, 1263.
37 S. Haq, J. G. Love, H. E. Sanders and D. A. King, *Surf. Sci.*, 1995, **325**, 230.
38 J. A. Anderson and C. H. Rochester, *J. Chem. Soc., Faraday Trans.*, 1986, **82**, 1911.
39 G. Li, M. J. Ridd and F. P. Larkin, *Aust. J. Chem.*, 1991, **44**, 623.
40 B. E. Hayden, A. King and M. A. Newton, *J. Phys. Chem. B*, 1999, **103**, 203.
41 L. Liao, W. Wu, C. Chen and J. Lin, *J. Phys. Chem. B*, 2001, **105**, 7678.
42 A. L. Goodman, E. B. Bernard and V. H. Grassian, *J. Phys. Chem. A*, 2001, **105**, 6443.
43 I. N. Tang and K. H. Fung, *J. Chem. Phys.*, 1997, **106**, 1653.
44 H. A. Al Abadleh, B. J. Krueger, J. L. Ross and V. H. Grassian, *Chem. Commun.*, 2003, **22**, 2796.
45 B. J. Krueger, V. H. Grassian, A. Laskin and J. P. Cowin, *Geophys. Res. Lett.*, 2003, **30**, 1148.
46 A. Laskin, T. W. Wietsma, B. J. Krueger and V. H. Grassian, *J. Geophys. Res.*, 2005, **110**, 1–15, DOI: 10.1029/2004JD005206, D10208.
47 W. Ostwald, *Z. Phys. Chem.*, 1897, **22**, 289.
48 J. Z. Schmelzer, *Phys. Chem.*, 1998, **204**, 171.
49 R. A. Van Santen, *J. Phys. Chem.*, 1984, **88**, 5768.
50 J. W. Morse and W. H. Case, *Am. J. Sci.*, 1988, **288**, 537.
51 B. Birkholz, B. Selle, W. Fuhs, S. Christiansen, H. P. Strunk and R. Reich, *Phys. Rev. B*, 2001, **64**, 085402-1.